Simulation of Off-Energy Electron Background in DELPHI

E. Falk, V. Hedberg
Department of Physics, University of Lund, Lund, Sweden
G. von Holtey
CERN

Abstract

Monte Carlo simulations of off-energy electron background in the DELPHI luminometer STIC are reported. The study simulates the running conditions at 68 GeV with and without bunch trains. The electrostatic separators, which create the vertical separation bumps for the bunch trains, cause a high concentration of background in the vertical plane. The simulations are compared to LEP data taken under similar running conditions. A comparison between the simulated running conditions at 68 GeV and those of the new LEP2 beam optics at 80.5 GeV is made. Moreover, the study investigates background components entering STIC elsewhere than through the front of the detector, and a significant portion is found to enter either from the back or from below. Possible improvements of the background situation are also discussed.

EUROPEAN ORGANIZATION FOR NUCLEAR RESEARCH

European Laboratory for Particle Physics

CERN - SL DIVISION

CERN SL/97-04(EA)

Simulation of Off-Energy Electron Background in DELPHI

E. Falk, V. Hedberg
Department of Physics, University of Lund, Lund, Sweden
G. von Holtey
CERN

Abstract

Monte Carlo simulations of off-energy electron background in the DELPHI luminometer STIC are reported. The study simulates the running conditions at 68 GeV with and without bunch trains. The electrostatic separators, which create the vertical separation bumps for the bunch trains, cause a high concentration of background in the vertical plane. The simulations are compared to LEP data taken under similar running conditions. A comparison between the simulated running conditions at 68 GeV and those of the new LEP2 beam optics at 80.5 GeV is made. Moreover, the study investigates background components entering STIC elsewhere than through the front of the detector, and a significant portion is found to enter either from the back or from below. Possible improvements of the background situation are also discussed.

Geneva, Switzerland
February 1997

1 Introduction

A simulation study of off-energy electron background in the DELPHI luminometer STIC has been carried out. The purpose of the simulation was to gain a better understanding of phenomena seen in data taken during the third running period (P3) of 1995. During this period, which took place in November 1995, LEP was operated at 68 GeV in bunch-train mode (albeit with only one and two wagons). This running period was the first in which the DELPHI experiment used a trigger aimed at selecting single-photon events in STIC. This so-called neutral trigger, which provides $e-\gamma$ separation, requires an energy deposit in one of the two STIC calorimeters in conjunction with an absence of signals in the scintillator planes in front of the calorimeters. It was immediately apparent that this trigger was very sensitive to off-energy electron background. Not only did off-energy electrons that entered STIC without passing the scintillation counters fire the trigger, but also electrons that arrived from the front did so because of counter inefficiencies.

Previously, the OPAL experiment reported an increase in off-energy electron background in their luminosity analysis when LEP began operating in bunch-train mode at 45 GeV [1]. A simulation of this background showed that an increase of the background in the vertical plane was due to the electrostatic separators that create the vertical separation bumps for the bunch trains of the counter-rotating beams in LEP.

In DELPHI, this background does not enter the sample of Bhabha events used in the luminosity measurement, because in this analysis only high-energy back-to-back electron-positron pairs are taken into account. The radial distribution of off-energy electrons is very steep, and since the inner acceptance for Bhabha electrons is at a larger radius in DELPHI than it is in OPAL, DELPHI also has a lower acceptance for off-energy electrons.

In single-photon analysis, however, DELPHI typically triggers on several thousand off-energy electrons for every true single-photon event. For this reason, a study of this background in DELPHI together with a simulation of off-energy electrons was carried out in order to investigate what the optimal running conditions of LEP may be, and also to determine whether the neutral trigger might be improved. The simulations were done at beam energies of 68 GeV and 80.5 GeV, imitating the running conditions of the third LEP period (P3) in 1995 and the first period (P1) in 1996.

2 STIC

The luminosity monitor STIC consists of two lead-scintillator calorimeters of shashlik type, read out by wavelength-shifting fibers. These are located on either side of the interaction point at a distance of 2.2 m [2]–[5]. The two calorimeters are usually referred to as arm A and arm C, according to the DELPHI convention of calling the side of incoming electrons side A and that of positrons side C; see Figure 1.

Each of the STIC calorimeters is equipped with two planes of silicon-strip detectors with which the direction of a shower can be measured. The purpose of this tracking device is to

improve rejection of off-energy electron background. A veto system consisting of two layers of scintillator is mounted in front of each arm of STIC. This veto system is part of the neutral trigger discussed above.

Several tungsten masks and shields are mounted on and near STIC. A so-called tungsten nose is mounted on the front face of the calorimeter on side C (but not on side A), and is used to define the acceptance for Bhabha electrons in luminosity measurements. A synchrotron radiation mask is mounted underneath each arm of STIC, inside the beam pipe, and these masks protect the DELPHI TPC from synchrotron radiation. Furthermore, a "tungsten shield", mounted on the tungsten nose, provides additional radiation protection to the TPC.

Figure 2 shows an outline of a STIC calorimeter with the silicon planes and the veto counters marked. The location of masks, nose and shields are also indicated. Each calorimeter is divided into 10 radial rings and 16 azimutal sectors, thus giving a total of 160 towers which point to the interaction region (see Figure 3). The dimensions of some of the beam-pipe components, the tungsten masks and the detectors are given in Table 1.

3 Simulation Program

The simulations were carried out with the CERN library program Decay Turtle [6], which simulates beams of charged particles through transport systems. It was modified both to include decay calculations that handle bremsstrahlung on residual gas molecules and to incorporate electrostatic separators in the beam transport line. A length of approximately 650 m of the LEP beam line was simulated, beginning at the quadrupole QF23 that lies 640 m upstream of the DELPHI interaction point. The program does not simulate energy loss in material, and any interaction with material results in full interception in this study.

The program assumes constant vacuum pressure (10^{-9} Torr) along the beam line. In reality, the vacuum pressure is known to differ between different sections of LEP and also within sections over time. Unfortunately, it is not possible to find out retroactively what the actual vacuum pressures were during a certain running period. The rate of off-energy electron background is proportional to the vacuum pressure.

The simulations were carried out at a beam energy of 68 GeV, with bump amplitudes of 50%, 80% and 100% of maximum amplitude of the vertical separation bump. (Maximum amplitude is obtained at voltages of 260 keV, 57 keV and 190 keV on the electrostatic separators ES.QS2, ES.QS4 and ES.QS7 respectively.) These conditions correspond to the LEP operating modes of fills 3182, 3183 and 3186 of November 1995, which are the fills that have been used for comparisons of the simulations with data. Simulations were also made with a beam energy of 80.5 GeV and a bump amplitude of 100%. This resembles the running conditions of period P1 of July–August 1996. 100% bump amplitude at 68 GeV beam energy corresponds to a maximum vertical displacement of the beam by 8.4 mm at the location of the quadrupole QS4. (The maximum beam displacement is inversely proportional to the beam energy and hence decreases for higher energies.) For comparison, simulations were also made without vertical separation bumps, again at 68 GeV. The layout of the vertical separation bump is shown in Figure 4.

The simulation set-up was chosen to imitate the electron beam coming in toward interaction point 8. The impact on the front plane of arm C of STIC was studied, both with and without the tungsten nose in front of the calorimeter; again, see Figures 1 and 2. This set-up corresponds to a negative bump polarity with a vertical axis pointing upwards. The opposite, *i.e.,* a positive bump polarity, is true for the positron beam hitting arm A, and the simulation of off-energy electron background of this arm is simply reversed with respect to the vertical axis compared to that of arm C.

Throughout the study, a cut was used to eliminate particles of energy less than 10 GeV. A similar cut was imposed on the STIC trigger, where events with reconstructed shower energies below 10 GeV were discarded.

4 Simulation: Comparison Between No Bump and Full Bump Amplitude

A comparison of the results of the 68 GeV simulations at zero and 100% bump amplitude shows several interesting features which appear when the electrostatic separators creating the bumps are switched on. Figure 5 shows plots of the shower energy deposited in the different calorimeter sectors for these two cases.

Without a vertical bump, the vast majority of the background is located in the horizontal plane. The energy spectrum shows a peak around 45 GeV with a tail towards lower energies. When the electrostatic separators are switched on, a large part of the background is shifted from the horizontal plane into the vertical plane. Peaks appear around 20 GeV in the lower part of the calorimeter and around 35 GeV in the upper part. Moreover, the background is clustered in a few relatively distinct groups. This grouping is related to where in the beam transport system the background was created, which will be discussed below. In order to facilitate a comparison with data, the following classification, illustrated in Figure 5 and in Table 2, was made: Particles entering sectors 1, 8, 9 and 16 belong to the horizontal group; particles entering sectors 11–14 belong to the vertical parallel group; and particles entering sectors 3–6 belong to the vertical antiparallel group. The names parallel and antiparallel refer to the direction of the deflection of the particles of these two groups with respect to that of the first deflection of the bunch-train bump. The vertical parallel group enters arm C in the upper part of the calorimeter and arm A in the lower part; the opposite is true for the antiparallel group.

4.1 Energy Distribution

The energy distributions with no bump and with full bump are shown for each of the three groups in Figure 6. These plots confirm the peaks that appear in Figure 5b when the electrostatic separators are switched on. They are centered at 46 GeV in the horizontal plane, at 22 GeV in the vertical antiparallel group and at 36 GeV in the vertical parallel group. A second peak at approximately 35 GeV also appears in the antiparallel group, as well as a long tail of

horizontal background with energies down to 10 GeV.

The two latter background components are clearly different from the main peaks of the horizontal and the vertical antiparallel groups respectively. Therefore, these two azimuthal groups were divided into a low-energy and a high-energy subgroup, with the division between the two at 25 GeV.

The high-energy component of the horizontal background seems relatively unaffected by the electrostatic separators, while the horizontal background swept into the vertical plane by the separators is mainly of lower energy.

4.2 Origin of Background

Each of the five groups described above originates from a specific part of the beam line upstream of the interaction point. Figure 7 shows the distances from the interaction point at which the backgrounds are created. The particles of the high-energy horizontal group are created beyond a distance of 106 m, or upstream of the quadrupole QS6. The high-energy vertical antiparallel group also originates from this part of the beam line, mainly immediately upstream of QS6. The low-energy horizontal group is created in the section between the interaction point and the electrostatic separator ES.QS2, located 24 m upstream of the interaction point. The low-energy antiparallel group originates from the region between ES.QS2 and the quadrupole pair QS3 and QS4, located 58.0 m and 64.2 m respectively upstream of the interaction point. Finally, the vertical parallel group is created in the section between QS3/QS4 and QS6.

4.3 Radial Distribution

The radial distribution also reveals interesting differences between the various groups, as Figure 8 shows. The radii are measured on the front face of the calorimeter. The distributions for the two horizontal groups extend from the inner edge of the calorimeter at 65 mm to approximately 110 mm, where the distributions are sharply cut. This is true both for a full vertical bump and for no bump at all. The sharp cut is the shadow of the synchrotron radiation mask *upstream* of the interaction point, *i.e.,* of the mask located inside the *opposite* arm of STIC. Simulations show that the radial distributions of the horizontal groups would extend to about 250 mm were it not for this mask.

The vertical groups, on the other hand, are not affected by the synchrotron radiation mask. The low-energy antiparallel group extends radially to over 200 mm, as does the parallel group. The upper radial limit for the high-energy antiparallel group is at approximately 150 mm.

The upper limit for the radial distribution is hardly affected by the presence of the vertical bump. The main difference in radial distribution is the relative occupancy of the different groups, the principal effect of the bump separators on the background being the transition from the horizontal to the vertical plane.

5 Comparison Between Data and MC

The simulated background has been compared to data taken during the 1995 P3 run at 136 GeV center-of-mass energy. Three fills have been studied, numbers 3182, 3183 and 3186, with bump amplitudes of 50%, 80% and 100% respectively. The last fill contains a small number of events, and the comparison presented here will concentrate on the other two fills. As discussed in Section 3, no interactions between the off-energy electrons and material were simulated. Detector effects causing a smearing in the energy and position measurements have also been ignored. All off-energy electrons in the simulation enter the calorimeter from the front, while in the data they may also enter STIC from behind or from below (*i.e.,* inside the hole for the beam pipe). This will be discussed further in Section 6. In addition, possible variations of the vacuum pressure during and between the data-taking periods have not been taken into account.

Despite the limitations of the Monte Carlo study, the data show clear evidence for all three major background components predicted by the simulation, as seen in Figures 9 and 10. The low-energy and the high-energy parts of the horizontal and the vertical antiparallel components are also present in the data, but, for the reasons given above, not necessarily with the same relative magnitude as in the simulation.

5.1 The Horizontal Background Component

In Section 4.3 it was pointed out that the Monte Carlo simulation has a sharp cut in the radial distribution at a radius of 110 mm due to the synchrotron mask. This cut is also clearly visible in the data (see Figures 11 and 12).

The histograms of the data from side C show many events having a reconstructed radius less than that of the tungsten nose and with an energy around 15 GeV. These events are of course not present in the simulation. A closer analysis of the data shows that these background electrons leave signals neither in the veto counter in front of the calorimeter nor in the silicon-strip detectors inside the calorimeter. Therefore, it is most likely that they enter STIC from behind or from below.

The two regions in the Monte Carlo energy distribution which are caused by electrons being created in different parts of LEP are also observed in the data. However, the high-energy peak seems to be less significant in the data than in the simulation. In the data, the low-energy peak overlaps with the peak from electrons coming from below and from behind; this background is peaked at a somewhat lower radius than the electrons entering from the front.

In the data from side A, which has no tungsten nose, there are many electrons with energies between the two peaks. Data from the veto counters show that these events typically have hits in a third or more of the sectors of the counters. This is an indication that these electrons come from the front, and that they have pre-showered before entering the calorimeter. Electrons entering STIC at low radii go through a very thick beam pipe (68 mm for electrons entering at the inner acceptance of STIC), and they also pass through a 44 mm thick beam-pipe flange and part of the beam-pipe bellows located nearby, which electrons entering STIC at higher radii do not (see Table 1). It is therefore likely that part of the high-energy background interacts with

the material at low angles and is detected in STIC at lower energies.

5.2 The Vertical Antiparallel Background Component

The simulation of the vertical antiparallel background shows distinct low-energy and high-energy groups in the radius-energy histograms, giving rise to two peaks in the energy distribution (see Figure 12). These groups are, as pointed out earlier, produced in different parts of LEP. These bands are also seen in the data (see Figure 11), where they are wider, probably because of the finite detector resolution. The relative number of events in the low- and the high-energy groups are different in data and in Monte Carlo, but this could be explained by the assumption of a constant vacuum pressure in LEP in the simulation. A higher pressure in a particular section of the beam line would give rise to more background electrons being created in that section.

Another difference between Monte Carlo and data is the presence in the latter of a low-radius band on side A (but not on side C). These events have multiple hits in the veto counters and are probably, as in the horizontal case, produced through interactions between high-energy electrons and material at low angles.

5.3 The Vertical Parallel Background Component

For the vertical parallel background component, the simulation predicts one band in the radius-energy plots with a broad peak at 30 GeV. This is in good agreement with the data (see Figures 11 and 12).

There is also a low-radius band with many veto-counter hits in the data from side A, and again, these events are most likely to be caused by interactions in and around the beam pipe.

6 Off-Energy Electrons Entering STIC Elsewhere than Through the Front

The sharp shadow of the upstream synchrotron radiation mask seen in simulations as well as in data indicates the possibility that off-energy electrons enter STIC upstream of the interaction point, *i.e.,* from behind. Electrons entering the calorimeter from behind would not leave a signal in the veto counters, and they would thus incorrectly fire the neutral trigger discussed in Section 2. Therefore, the radial distribution of each of the background groups was studied in detail at certain points along the beam line. The points were chosen as illustrated with arrows in Figure 13, so that they would correspond to: particles entering arm A either from behind or from below; particles entering arm C either from the front face or from below; particles escaping through the gap between STIC and the synchrotron radiation mask on side A and then hitting the front face of arm C; and particles being stopped by one of the two synchrotron radiation masks. Particles reaching the front face of arm C were treated separately depending on the radius being larger or smaller than that of the tungsten nose. The simulations were carried

out with a beam energy of 68 GeV, at 50% and 100% bump amplitudes, and the results are illustrated in Figures 13 and 14 respectively.

6.1 Background Entering STIC From the Front

With a bump amplitude of 50%, about 84% of the particles entering STIC enter from the front. Of these, 8% enter STIC in the hole for the beampipe, *i.e.,* below the tungsten nose. With all groups combined, 45% of the particles entering STIC enter the front face in the region covered by the tungsten nose. Most of these belong to the horizontal groups, which are concentrated below 110 mm in radius due to the shadow of the synchrotron radiation mask. As a result, the horizontal background on side C is almost entirely stopped by the tungsten nose, and the vertical background becomes dominant instead.

6.2 Background Entering STIC From the Back

Most of the particles entering from the back, about 3/4 at 50% bump amplitude, belong to the high-energy horizontal group. No particles of the high-energy antiparallel group and hardly any of the parallel group enter STIC in this way. Particles that enter STIC in ways other than through the front face do not follow the projective geometry of STIC. When this happens, the energy is not necessarily correctly reconstructed in the off-line data processing; in fact, the calculated energy may well be too low. Since a large part of the background concerned comes from the high-energy horizontal group, this could account for some of the difference in quantity between data and simulation seen in the low-energy horizontal group.

About 6% of the particles entering STIC pass between the calorimeter and the synchrotron radiation mask on side A and enter the front face of arm C at a radius of approximately 150 mm, *i.e.,* above the tungsten nose.

6.3 The Synchrotron Radiation Mask

In addition to the above, about 18% as many particles as enter STIC hit the synchrotron radiation mask from the back and about 30% hit the mask from the front at 50% bump amplitude. Those being stopped by the mask on side A belong almost exclusively to the horizontal groups, and simulations without the mask show that they would all have entered the front of side C had the mask not been there. On the other hand, those particles which are stopped by the mask on side C would not have entered the calorimeter in the absence of the mask. However, it is possible that some of the energy of these particles leaks into the calorimeter from underneath; due to the limitations of the simulations, it is beyond the scope of this study to resolve this question.

7 LEP2

Between 1995 and 1996, LEP underwent major upgrades, and the beam energy was increased from 68 GeV at the end of 1995 to 80.5 GeV during the first running period of 1996. The effects of these machine modifications to the background situation were investigated through simulations of the new beam optics with a beam energy of 80.5 GeV. The only significant effect observed is an increase of the background energy, which scales linearly with the beam energy for each of the different background groups (see Figure 15). The qualitative behavior of these groups, and in particular, their radial distributions, remain practically unaltered.

8 Can the Off-Energy Electron Background be Reduced?

8.1 LEP Running Conditions

The exposure of STIC to off-energy electrons can be reduced by closing the nearest collimators, vertical COLV.QS1 and/or horizontal COLH.QS1, and by changing the amplitude of the vertical separation bump.

Closing the vertical collimator COLV.QS1 would reduce the vertical parallel and the vertical antiparallel high-energy background below a collimator half-opening of 40 mm, as shown in Figure 16. The standard setting used for COLV.QS1 in 1995 was 33 mm, which reduced the background rates from these two groups by approximately 30%. In 1997, this collimator will be moved from its present location at 8.5 m from the interaction point upstream to a new location at 15 m from the interaction point, where it will be called COLV.QS2. The effect of closing the collimator in its new location is shown in Figure 17. Here, the collimator must be closed to below 20 mm before it begins to have any effect on the rate of vertical background. On the other hand, the beam is also much narrower, and it would be possible to close the collimator to perhaps 13 mm. This would reduce the rate of vertical background by about 50%. (In order to ensure that the collimators do not scrape the tails of the beam, they should not be closed further than to 30 σ_y. The beam size σ_y is 0.8 mm at the old location of the collimator and will be 0.41 mm at the new location, assuming an emittance of 3.3 nm.)

The amount of high-energy horizontal background begins to decrease at a half-opening of collimator COLH.QS1 of 35 mm and is reduced by 50% at a half-opening of about 17 mm, as shown in Figure 18. The setting used in 1995 was 32 mm. In this case it does not seem possible to reduce the background by closing the collimator.

At a beam energy of 68 GeV, the amplitude of the vertical separation bump must be below about 50% in order to decrease the amount of high-energy vertical background significantly, as shown in Figure 19. Reducing the bump amplitude of course also increases the horizontal background, since the bump amplitude does not affect the amount of background created (or even that reaching STIC), but only the fraction swept into the vertical plane. In the case of the vertical parallel background, which is the most disturbing kind in the physics analysis, the amplitude must be less than 20% for a reduction of a factor of two in rate. At present, it

is not known how small a bump amplitude can be used without beam-beam effects becoming disturbing, but the bump amplitude is probably not an effective tool in the fight against this background.

One issue which is of great importance is the quality of the vacuum in LEP and in particular in those regions in which the high-energy vertical background is produced, *i.e.,* in the regions between the quadrupoles QS7 and QS3. During 1996, for example, the rate of vertical background in the 172 GeV running period was ten times lower than that in the previous 161 GeV running period. It is most likely that this was due to an improved vacuum during the later part of the year, because the beam itself slowly cleans the vacuum. The vacuum was broken in the section between the quadrupoles QS2 and QS4 during the winter shutdown of 1996-1997. This is the section where low-energy vertical antiparallel background is produced, and one may therefore expect a higher rate of such background at the startup in 1997.

8.2 Improvements of STIC

From the radius-energy distributions in Figures 11 and 12 it is clear that an effective method to reduce the background is to apply a radial cut. With a cut at a radius of 12 cm, all horizontal and most of the vertical background is removed. The energy of the remaining vertical background is less than 35 GeV, which is about half the beam energy.

Since a radial cut reduces the background very efficiently, the STIC neutral trigger was modified in 1996 between the 161 GeV and the 172 GeV running periods to allow for a crude radius measurement to be made on-line and used in the trigger decision.

New scintillation counters, so-called small veto counters, covering low angles were also added to the experiment in 1996, and were incorporated in the neutral trigger in order to reduce the trigger rate further and to close a hole which appeared in the old veto-counter system when the tungsten nose was replaced by a smaller tungsten shield in 1996.

One possible additional improvement would be to cover part of the back of the calorimeter with some shielding in order to reduce the amount of horizontal background entering this way. The space available at the back is limited, however, and this type of background is easily rejected off-line with the silicon-strip detectors discussed in Section 2. The new on-line radius cut should also reduce the trigger rate.

9 Summary and Conclusions

The results of the simulation of off-energy electron background in STIC can be summarized in the following way:

- The background appears in distinct groups. This grouping is related to where in the beam line the background has its origin, and the behavior of the groups depends on the amplitude of the vertical bunch-train bump created by the electrostatic separators. Five different groups have been defined: two groups which enter STIC in the horizontal plane,

one of which is of higher energy (peaked around 45 GeV at a beam energy of 68 GeV) and one of lower energy (10–25 GeV); a vertical group deflected in the direction parallel to that of the bunch-train bump, which enters STIC in the upper part of side A and in the lower part of side C and which is peaked in energy around 35 GeV; and two vertical groups antiparallel to the bump, one of higher energies (peaked at 35 GeV) and one of lower energies (peaked at 15 GeV).

- There is good agreement between the Monte Carlo and data taken during P3 in 1995. All five groups identified above are seen in the data. The groups have similar energy and radius distributions. The shadow of the synchrotron radiation mask is very sharp both in simulations and in the data. The radius-energy distributions (Figures 11 and 12) show that there is a low-radius band of electrons in the data from side A which is not present in the simulations. This band is most likely to be caused by interaction with material traversed by electrons entering STIC at low angles. Moreover, the simulations do not agree with the data on the relative population of the different groups. A possible explanation for these discrepancies lies in the differences in vacuum pressure between different parts of the beam line, which are not accounted for in the simulation.

- A significant portion (some 25%) of the off-energy electron background which hits STIC enters the detector elsewhere than through the front. Most of this background enters from the back, and a large fraction thereof comes from the high-energy horizontal group. Since these particles do not follow the projective geometry of STIC, their energy is not necessarily correctly reconstructed in the off-line data processing. This could account for some of the relative abundance of low-energy horizontal background seen in data but not in Monte Carlo.

- The modifications of the beam optics for LEP2 that were made between 1995 and 1996 have not altered the qualitative behavior of the off-energy electron background. The energy of the background scales linearly with the beam energy.

- It is possible to reduce the rate of vertical high-energy background by closing the vertical collimator COLV.QS1. In 1997, when this collimator is placed at a new location further upstream, one may be able to reduce this background by 50% by closing it to 13 mm. On the other hand, closing the horizontal collimator COLH.QS1 enough to reduce the rate of horizontal background is not possible. Nor is reducing the bunch-train bump amplitude an efficient tool to improve the situation. The most important factor concerning operation of LEP, however, is the quality of the vacuum in the region of the electrostatic separators. Due to an opening of the section between quadrupoles QS2 and QS4, the rate of low-energy vertical antiparallel background is expected to increase at the startup of 1997.

- The STIC neutral trigger was improved during 1996 by the addition of new low-angle scintillator counters and the inclusion of a radius requirement in the trigger decision. However, the off-energy background remains the most serious problem in single-photon analysis.

10 Acknowledgements

The authors wish to thank I. Belokopytov, M. Lamont and E. Migliore, who helped us retrieve information from the DELPHI and LEP databases for P3 1995. We also appreciate fruitful discussions with T. Camporesi.

References

[1] G. von Holtey, *Off-Energy Electron Background with Bunch Trains in LEP,* CERN SL/95-86 (EA).

[2] S. J. Alvsvaag et al., *The Small Angle Tile Calorimeter project in DELPHI,* DELPHI 95-12 CAL 119, Contribution to the 4th International Conference on Advanced Technology and Particle Physics, Como, Italy, October 1994.

[3] S. J. Alvsvaag et al., *The DELPHI Small Angle Tile Calorimeter,* DELPHI 94-157 CAL 120, Contribution to the IEEE 1994 Nuclear Science Symposium and Medical Imaging Conference, Norfolk, USA, October 1994.

[4] S. J. Alvsvaag et al., *The new small angle calorimeter in DELPHI,* DELPHI 94-148 CAL 118, Contribution to the 5th International Conference on Calorimetry, Brookhaven, USA, September 1994.

[5] S. J. Alvsvaag et al., *The DELPHI Small Angle Tile Calorimeter,* DELPHI 95-14 CAL 123, Contribution to the Beijing Calorimetry Symposium, Beijing, China, October 1994.

[6] K. L. Brown, Ch. Iselin, *DECAY TURTLE—A Computer Program for Simulating Charged Particle Beam Transport Systems, Including Decay Calculations,* CERN 74-2.

Component	Radial coverage (in mm)	Polar angular coverage (in mrad)
Aluminium beam pipe	$53 \leq r \leq 55$	$\theta \leq 30$
Steel beam pipe	$53 \leq r \leq 55$	$\theta \geq 29$
Beam-pipe bellows	$55 \leq r \leq 66$	$26 \leq \theta \leq 35$
Beam-pipe flange	$55 \leq r \leq 73$	$29 \leq \theta \leq 40$
Synchrotron mask	$41 \leq r \leq 53$	$17 \leq \theta \leq 23$
Tungsten nose	$60 \leq r \leq 96.173$	$29 \leq \theta \leq 44.1$ [1]
Veto counters	$87.8 \leq r \leq 379$	$44 \leq \theta \leq 185$
STIC scint. planes	$65 \rightarrow 76 \leq r \leq 417.5$ [2]	$29.5 \leq \theta \leq 188 \rightarrow 161$ [3]
STIC lead planes	$65 \leq r \leq 417.5$ [4]	$29 \rightarrow 25 \leq \theta \leq 188 \rightarrow 161$ [3]
Si strip planes	$71.5 \rightarrow 73.2 \leq r \leq 174.2 \rightarrow 178.4$ [5]	$32 \leq \theta \leq 77$

Table 1: The dimensions of beam-pipe components, tungsten masks and STIC detectors.

AZIMUTHAL REGION	SIDE A		SIDE C	
	STIC sectors	Azimuthal angle	STIC sectors	Azimuthal angle
Horizontal	1+16 8+9	$0° \pm 22.5°$ $180° \pm 22.5°$	1+16 8+9	$0° \pm 22.5°$ $180° \pm 22.5°$
Vertical parallel	3+4+5+6	$90° \pm 45°$	11+12+13+14	$270° \pm 45°$
Vertical antiparallel	11+12+13+14	$270° \pm 45°$	3+4+5+6	$90° \pm 45°$

Table 2: Definitions of horizontal, vertical parallel and vertical antiparallel azimuthal regions. The azimuthal angle is defined in a coordinate system with the x axis pointing to the center of LEP, the y axis upwards and the z axis in the direction of the electron beam (*i.e.,* towards calorimeter C). The numbering of STIC sectors is such that sectors 1 and 16 are on the side nearest the LEP center, sectors 3-6 are in the upper half of the calorimeters and sectors 11-14 in the lower half.

[1] This corresponds to a radius ≤ 97.019 mm at the first scintillator plane.
[2] The inner radius is given for the first and the last scintillator plane in the calorimter.
[3] The value before the arrow refers to the first sandwich plane and the value after the arrow to the last plane.
[4] All the lead converter plates have the same size.
[5] The value before the arrow refers to the first Si strip plane and the value after the arrow to the last plane.

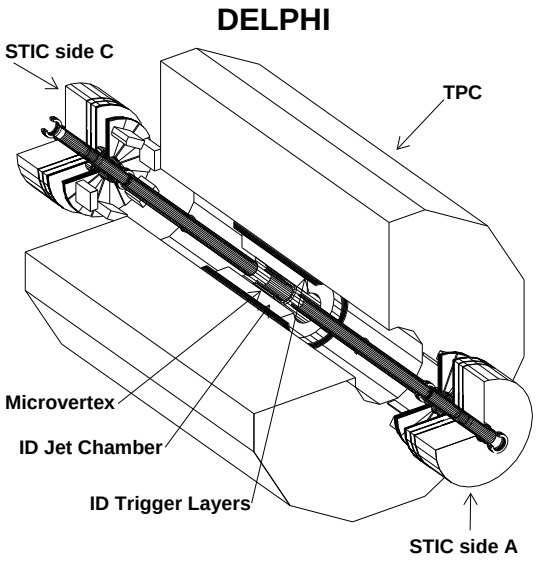

Figure 1: Location of STIC inside DELPHI. The STIC calorimeters are placed at a distance of 2.2 m on either side of the interaction point. Side A is that of the incoming beam of electrons; side C that of the incoming positrons. The electron beam has negative separation-bump polarity at this interaction point, and the positron beam has positive polarity.

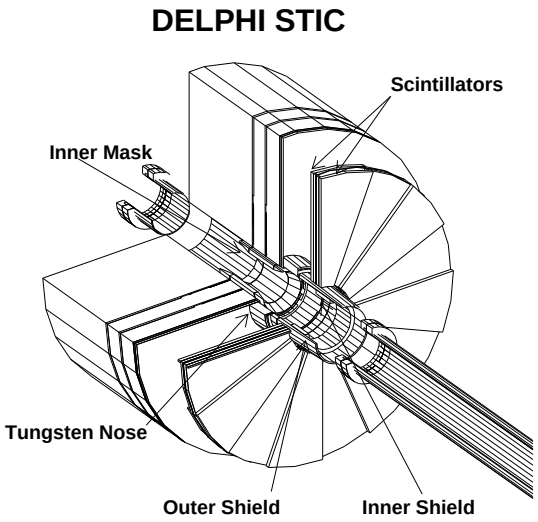

Figure 2: Outline of a STIC calorimeter showing the two scintillator planes of the veto counters in front of the calorimeter and the two planes of silicon detectors inside it. The tungsten nose and the synchrotron radiation mask, or inner mask, are marked. The position of the synchrotron radiation mask indicated here is that of 1994; in 1995 it was placed further back.

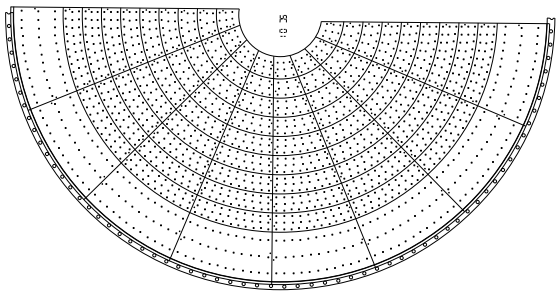

Figure 3: One half of the first STIC sandwich layer. Each calorimeter is divided into 10 radial rings and 16 azimuthal sectors, giving a total of 160 towers which point to the interaction region. The convention in numbering the calorimeter sectors is to use numbers 1–16 starting just above the horizontal plane on the inside of the LEP ring, and passing via the upper half of the calorimeter through the outside of the ring and onto the lower calorimeter half.

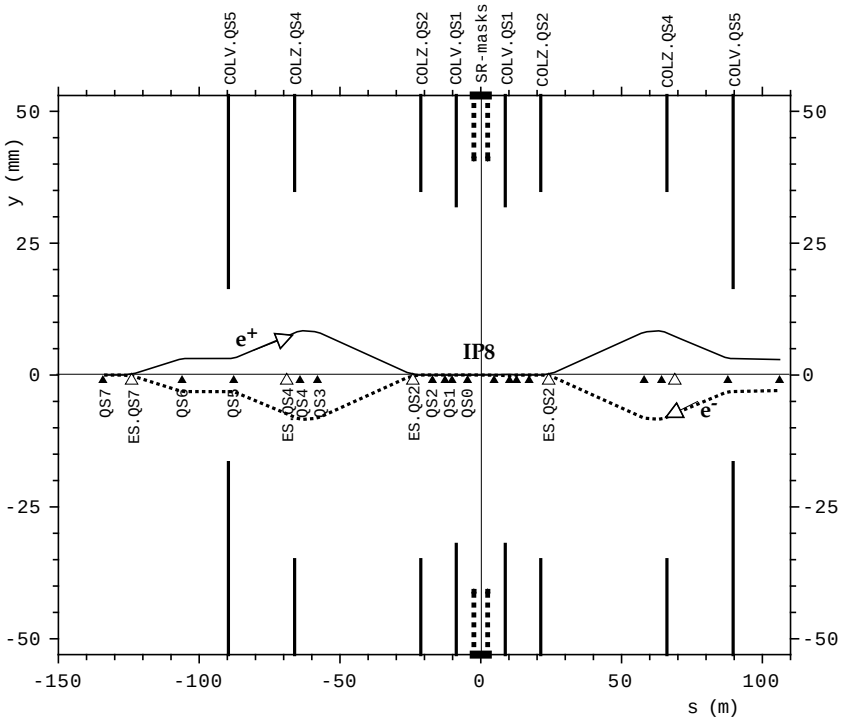

Figure 4: Layout of the vertical separation bump at the DELPHI interaction point (IP8). The bump amplitude reaches its maximum at quadrupole QS4 and is 8.4 mm for a beam energy of 68 GeV.

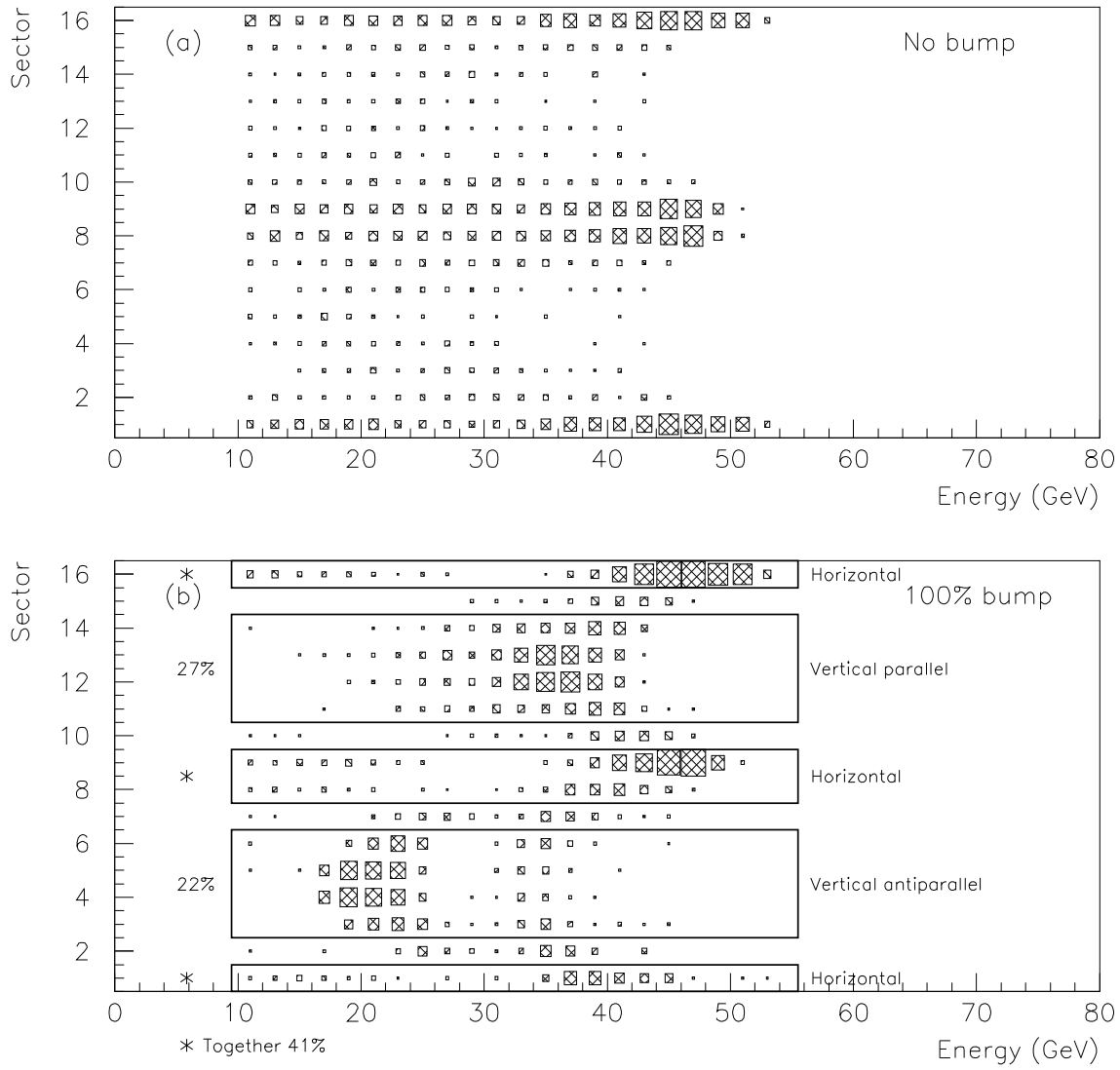

Figure 5: Comparison between (a) simulation with no separation bump and (b) simulation with 100% separation bump at 68 GeV beam energy for arm C without the tungsten nose. The histograms show calorimeter sectors *vs.* calorimeter energy. The areas of the boxes are proportional to the number of entries in the corresponding histogram bin. The names "parallel" and "antiparallel" refer to the direction of the deflection of the particles of these two groups with respect to that of the first deflection of the bunch-train bump.

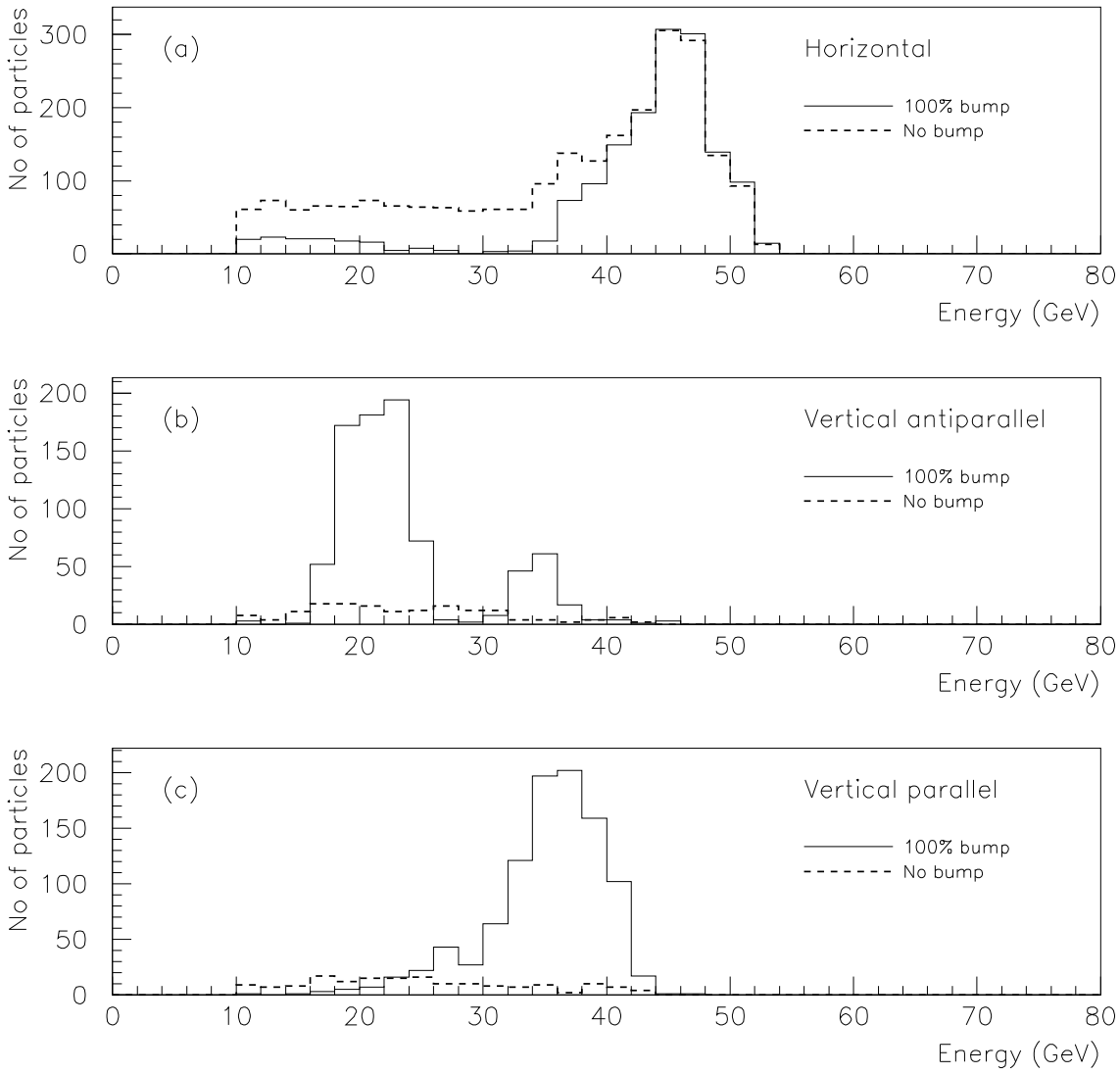

Figure 6: Simulated energy distributions with and without bunch-train bump at 68 GeV for (a) the horizontal group, (b) the vertical antiparallel group, and (c) the vertical parallel group.

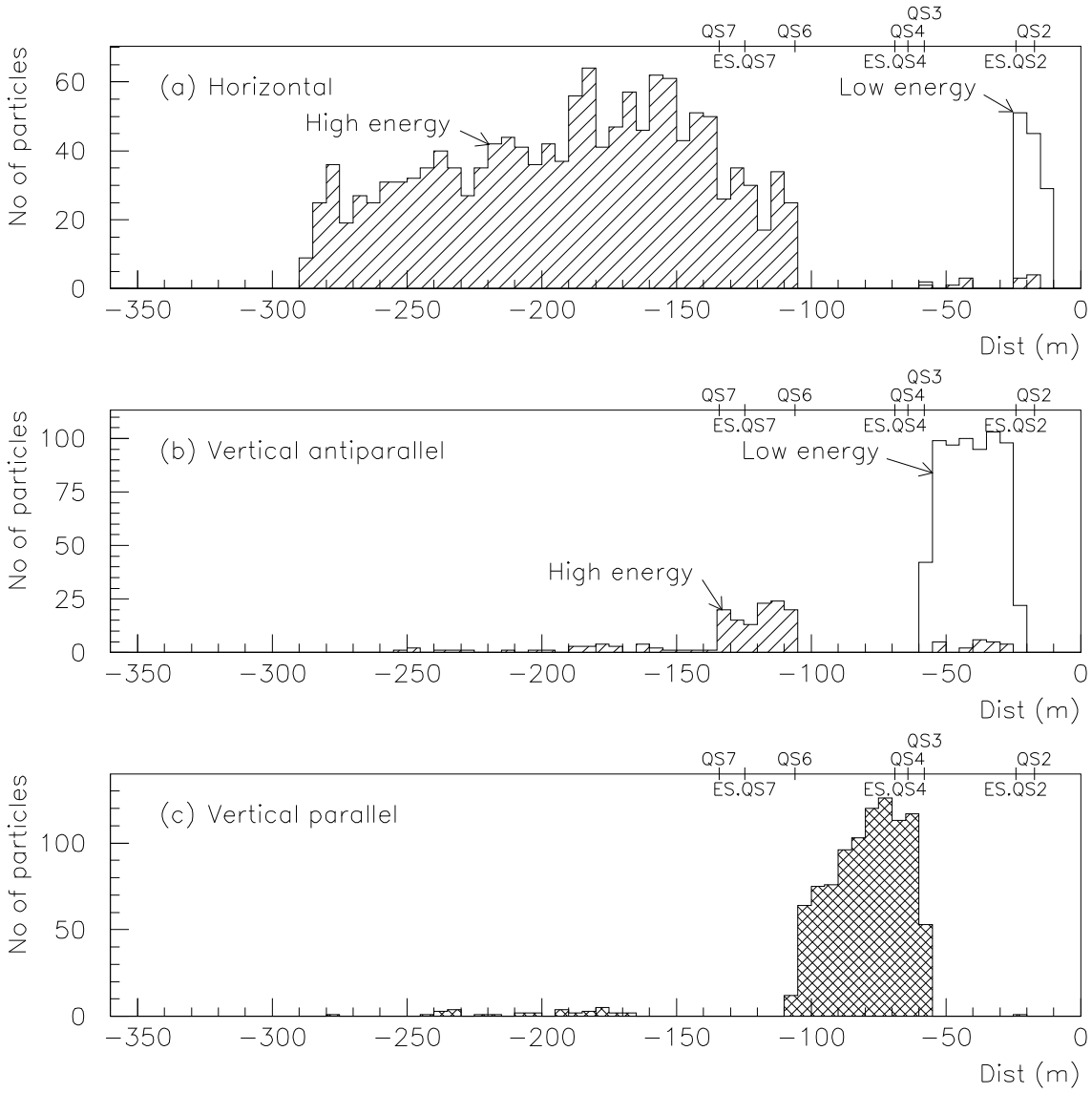

Figure 7: Distance from interaction point at which background was created for different background groups. The simulation was made with 100% bump amplitude at 68 GeV. The locations of the electrostatic separators (ES.QS2, ES.QS4 and ES.QS7) and nearby quadrupoles (QSn) are marked.

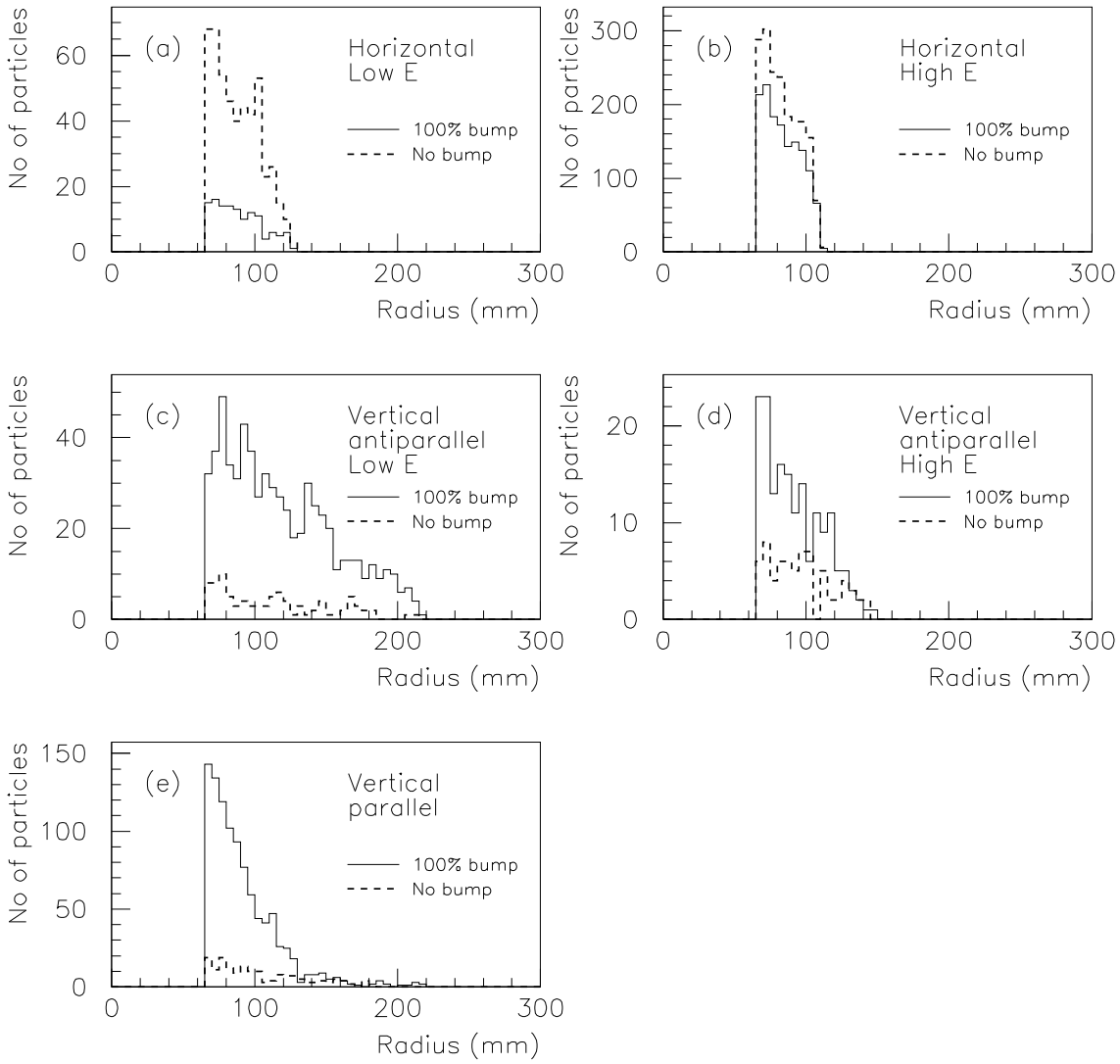

Figure 8: Radial distribution of different background groups at the front face of arm C, without the tungsten nose, both with and without the bunch-train bump. STIC extends radially from 65 mm to 417.5 mm. Note the sharp shadow of the synchtrotron radiation mask at 110 mm in the horizontal groups.

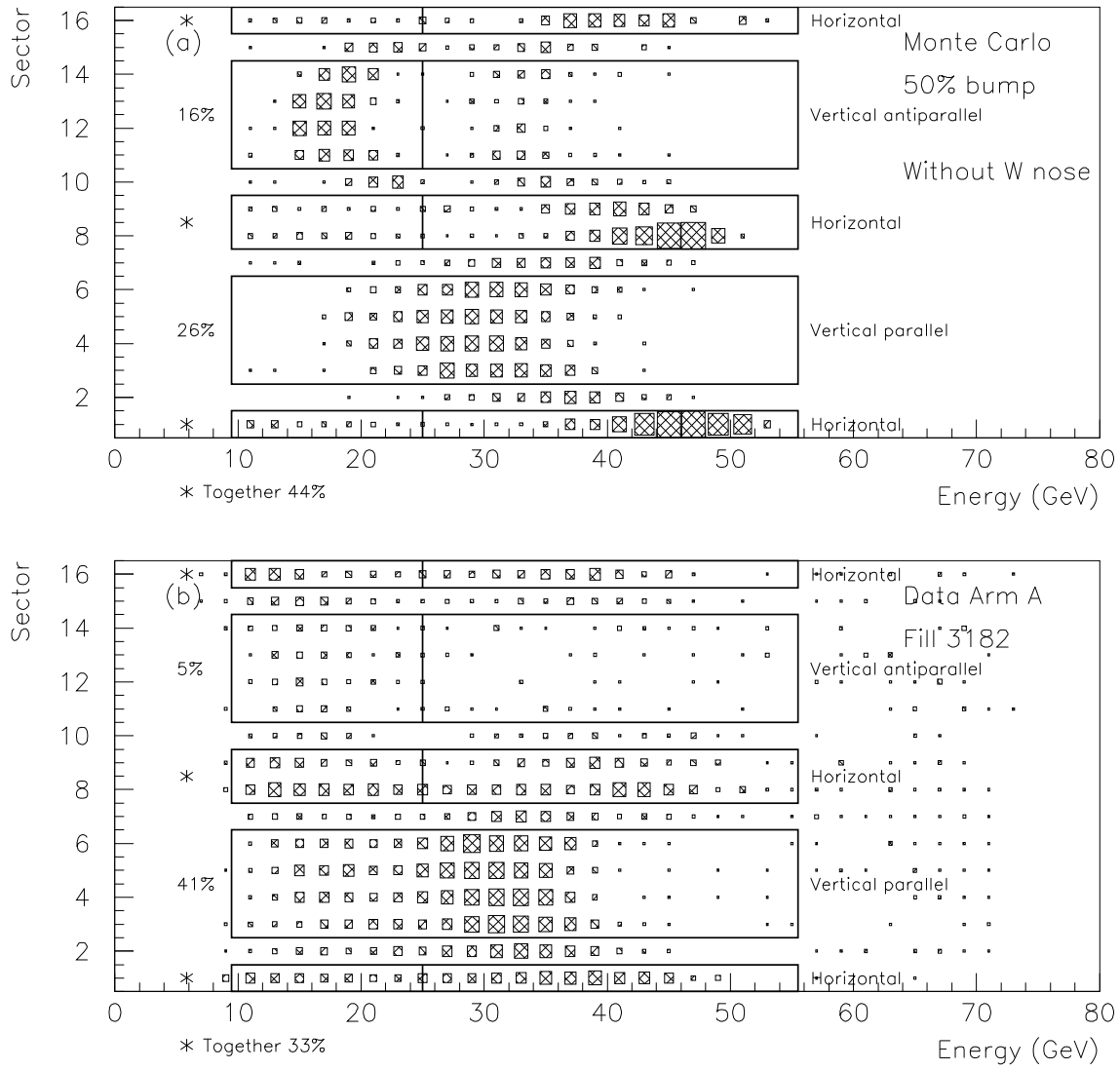

Figure 9: Comparison of calorimeter sector *vs.* energy between (a) Monte Carlo without the tungsten nose, and (b) data for arm A at 68 GeV beam energy and 50% bump amplitude. The vertical lines mark the division between low-energy and high-energy groups. The histograms have been normalized to have the same number of entries.

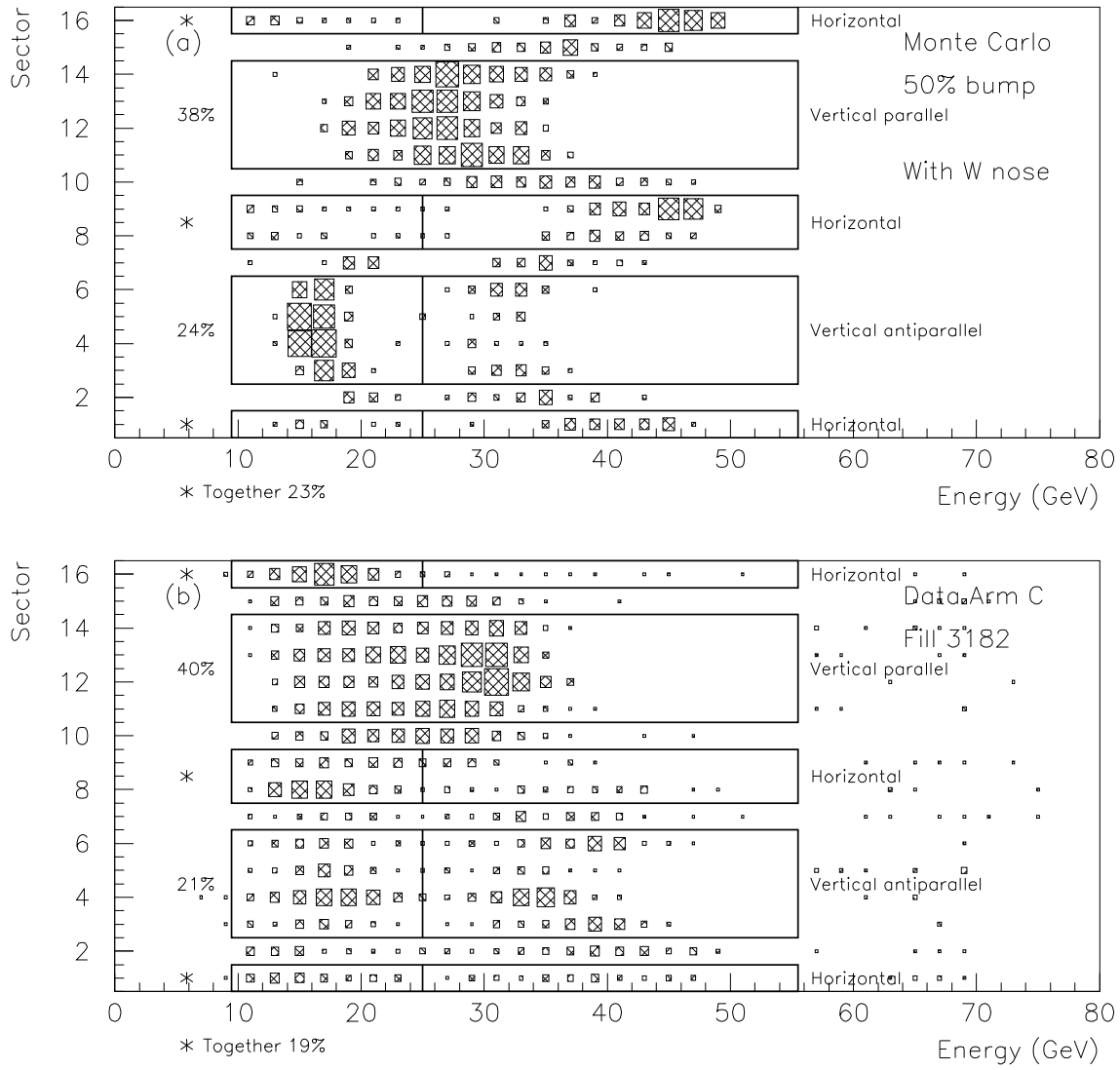

Figure 10: Comparison of calorimeter sector *vs.* energy between (a) Monte Carlo with the tungsten nose, and (b) data for arm C at 68 GeV beam energy and 50% bump amplitude. The vertical lines mark the division between low-energy and high-energy groups. The histograms have been normalized to have the same number of entries.

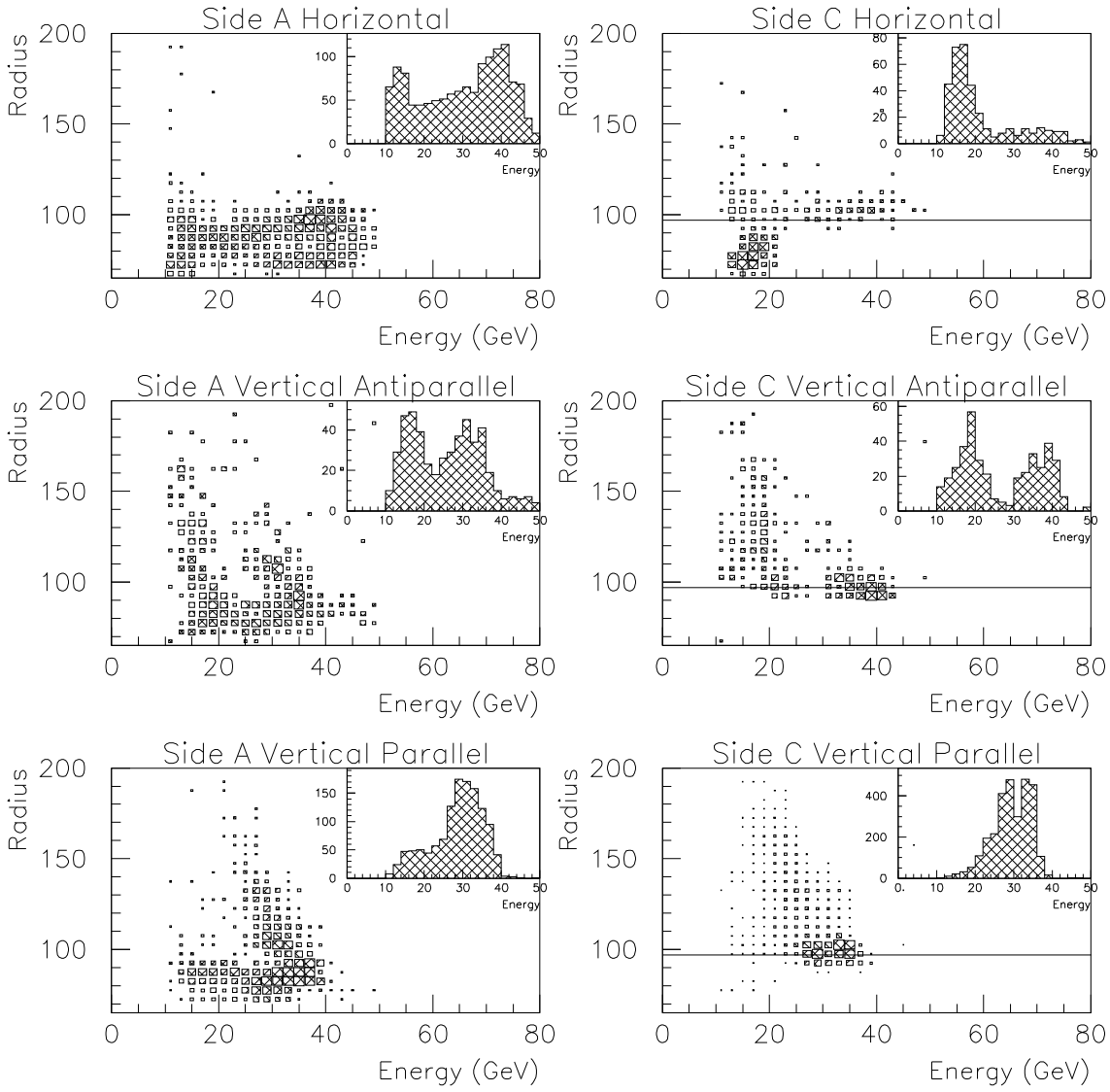

Figure 11: Distribution of radius *vs.* energy of off-energy electrons in data at an energy of 68 GeV per beam and at a bump amplitude of 80% for different background groups. The horizontal line in the histograms for side C indicates the position of the edge of the tungsten nose.

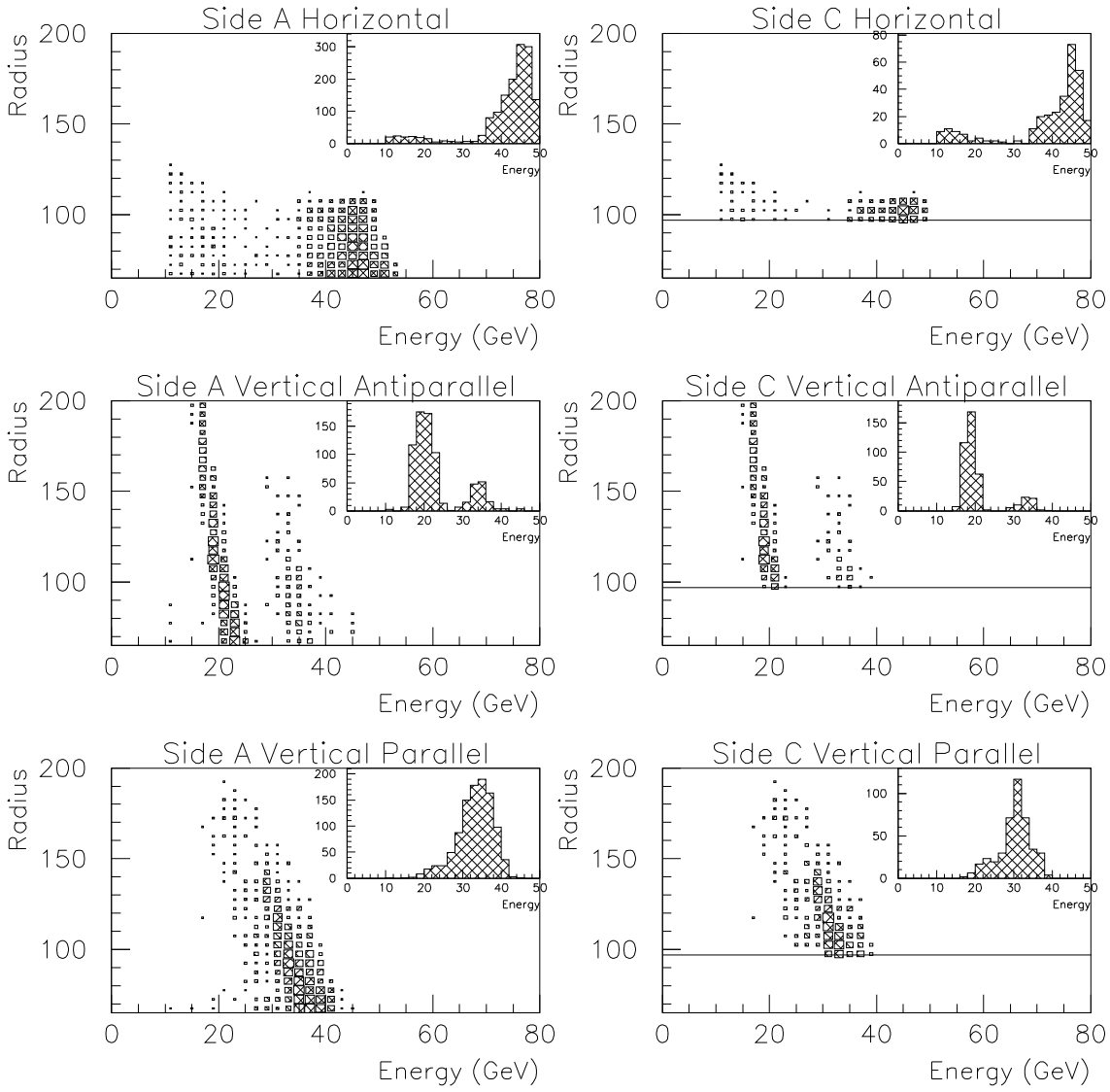

Figure 12: Simulated distribution of radius *vs.* energy of off-energy electrons at an energy of 68 GeV per beam and at a bump amplitude of 80% for different background groups. The horizontal line in the histograms for side C indicates the position of the edge of the tungsten nose.

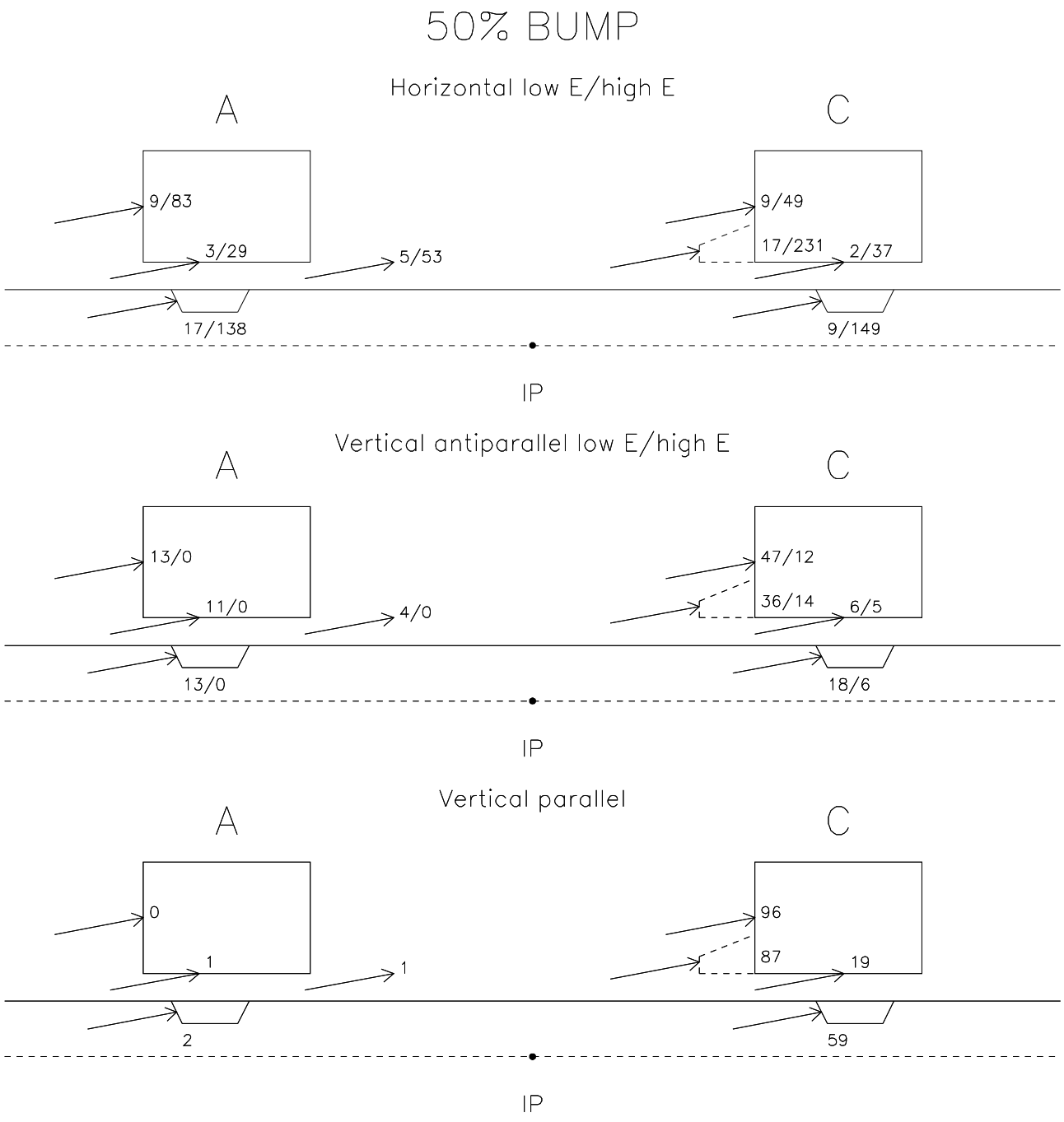

Figure 13: Different entry points for off-energy electrons entering STIC. (Only the electron beam was simulated.) The numbers in the figure show the number of particles entering at each point from each background category at 68 GeV beam energy and at 50% bump amplitude and normalized to a total of 1000 particles *entering* STIC. Particles hitting the synchrotron radiation masks are thus in addition to these 1000 particles. However, the sum of the number of particles entering STIC from each of the groups in the figure is not 1000; this is due to the definition of the groups, which leaves out certain calorimeter sectors.

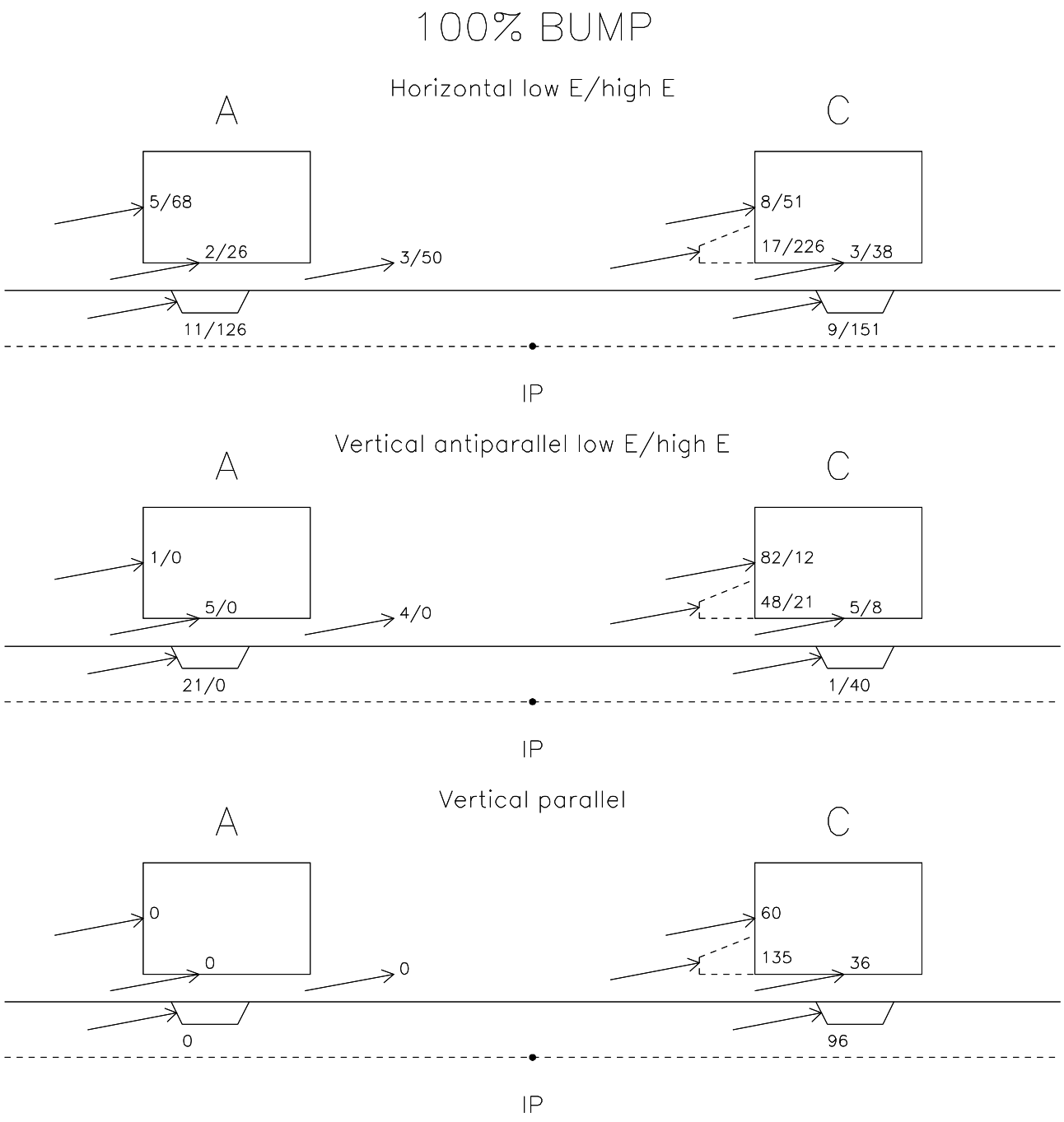

Figure 14: Different entry points for off-energy electrons entering STIC. The numbers in the figure show the number of particles entering at each point from each background category at 68 GeV beam energy and 100% bump amplitude and normalized to a total of 1000 particles *entering* STIC.

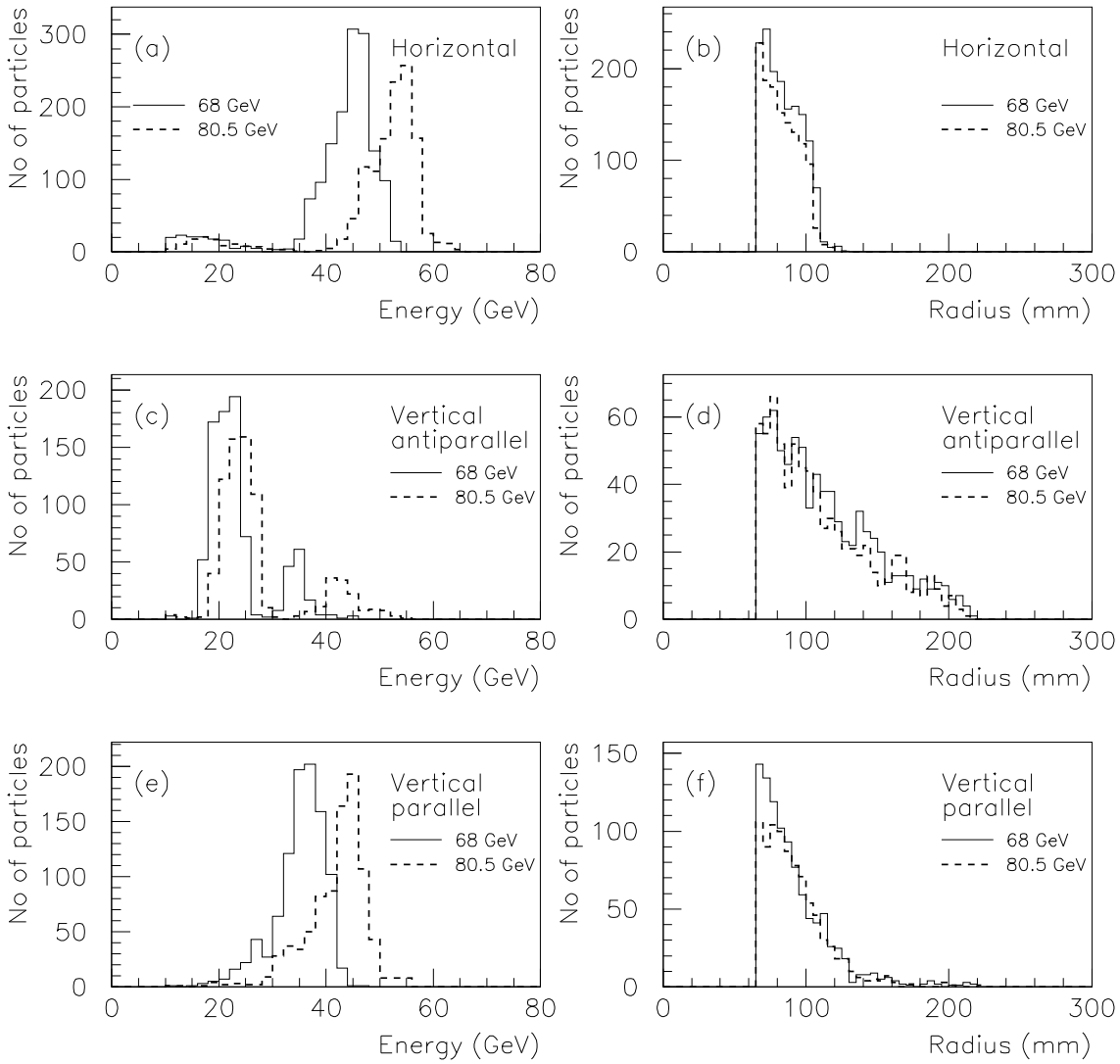

Figure 15: Comparison of simulated energy distributions and radial distributions between the beam optics of 1995, with a beam energy of 68 GeV, and that of 1996, with a beam energy of 80.5 GeV, for different background groups.

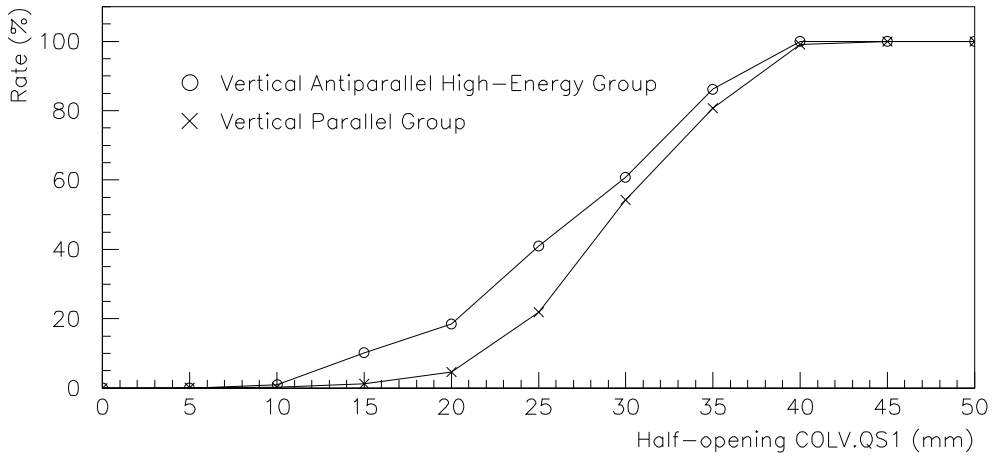

Figure 16: Rate of background of the vertical antiparallel high-energy group and of the vertical parallel group as a function of the half-opening of the vertical collimator COLV.QS1. The standard half-opening used in 1995 was 33 mm. The rates are normalized to those of a half-opening of 50 mm.

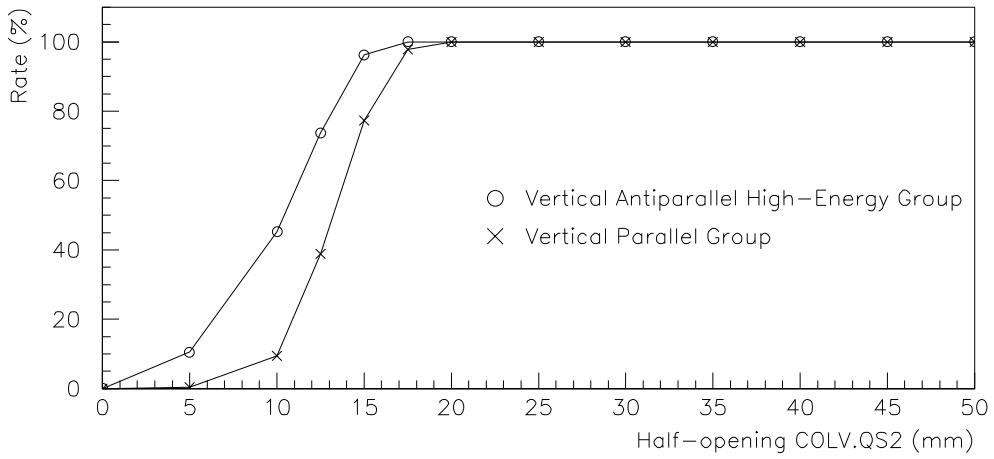

Figure 17: Rate of background of the vertical antiparallel high-energy group and of the vertical parallel group as a function of the half-opening of the old vertical collimator COLV.QS1 in its new position for 1997, where it will be called COLV.QS2. The rates are normalized to those of a half-opening of 50 mm.

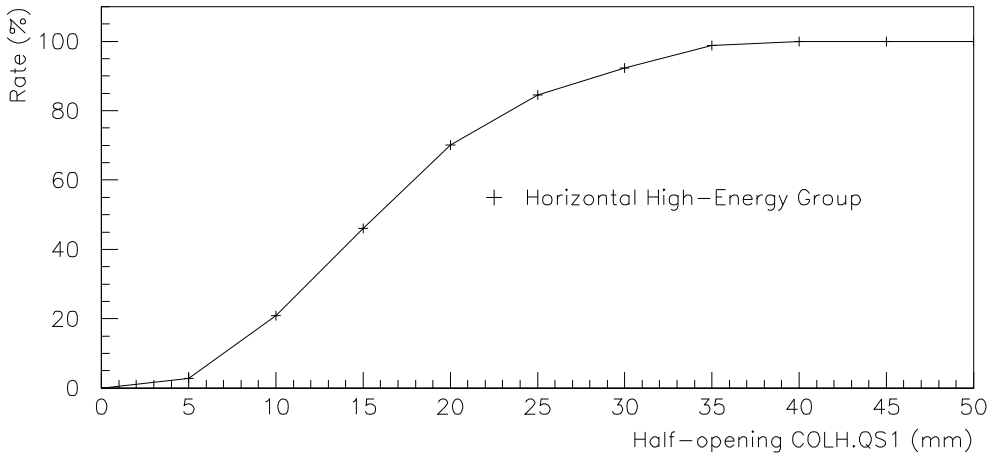

Figure 18: Rate of background of the horizontal high-energy group as a function of the half-opening of the horizontal collimator COLH.QS1. The standard half-opening used in 1995 was 32 mm. The rate is normalized to that of a half-opening of 50 mm.

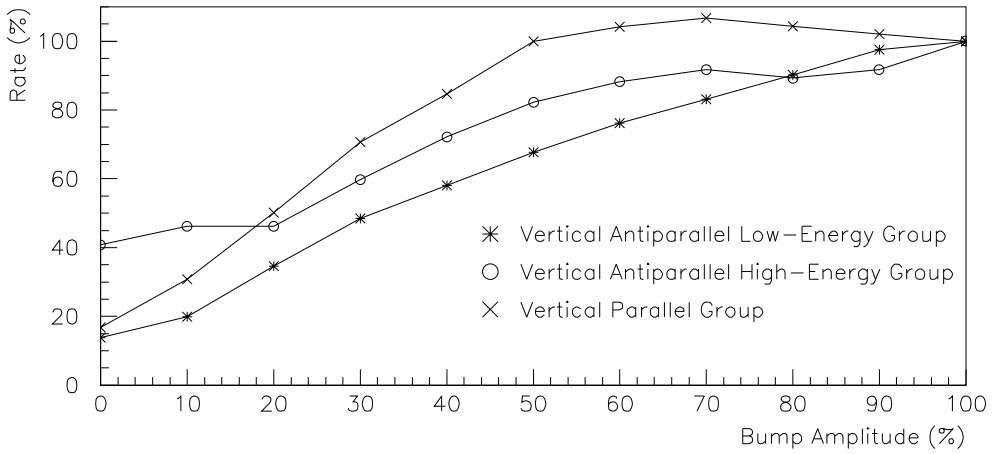

Figure 19: Rate of background in the vertical plane as a function of the amplitude of the vertical separation bumps for different background groups. The bump amplitude is given as a percentage of maximum amplitude at 68 GeV beam energy. The rates are normalized to those of 100% bump amplitude.